Coupled molecular-dynamics and finite-element-method simulations for the kinetics of particles subjected to field-mediated forces

Michele Cascio,[1,2,3] Davide Baroli,[4] Stephane Bordas,[4] Ioannis Deretzis,[2] Giuseppe Falci,[1,3] Antonino Magliano,[2] and Antonino La Magna[2]

[1]*Department of Physics and Astronomy, University of Catania, Via S. Sofia 64, 95123 Catania, Italy*

[2]*CNR-IMM, Z.I. strada VIII 5, 95121 Catania, Italy*

[3]*INFN-Catania, Via S. Sofia 62, 95123 Catania, Italy*

[4]*Institute of Computational Engineering, University of Luxembourg, Maison du Nombre 6, Avenue de la Fonte, L-4364 Esch-sur-Alzette, Luxembourg*

(Received 31 July 2018; published 17 June 2019)

A computational approach that couples molecular-dynamics (MD) and the-finite-element-method (FEM) technique is here proposed for the theoretical study of the dynamics of particles subjected to electromechanical forces. The system consists of spherical particles (modeled as micrometric rigid bodies with proper densities and dielectric functions) suspended in a colloidal solution, which flows in a microfluidic channel in the presence of a generic nonuniform variable electric field generated by electrodes. The particles are subjected to external forces (e.g., drag or gravity) which satisfy a particlelike formulation that is typical of the MD approach, along with an electromechanical force that, in turn, requires the three-dimensional self-consistent solutions of correct continuum field equations during the integration of the equations of motion. In the MD-FEM method used in this work, the finite element method is applied to solve the continuum field equations while the MD technique is used for the stepwise explicit integration of the equations of motion. Our work shows the potential of coupled MD-FEM simulations for the study of electromechanical particles and opens a double perspective for implementing (a) MD away from the field of atomistic simulations and (b) the continuum-particle approach to cases where the conventional force evaluation used in MD is not applicable.

DOI: 10.1103/PhysRevE.99.063307

I. INTRODUCTION

Particles with sizes that range from submicrometers to about 1 mm and with particular electrical and/or magnetic properties experience mechanical forces and torques when they are subjected to electromagnetic fields; particles of this type are called "electromechanical particles" (EMPs) [1]. Mutual interactions between EMPs could also occur when they are close enough to modify the force field obtained in the isolated particle limit. Consequently, away from the isolated particle (diluted) limit, EMPs behave like complex many-particle systems whose stable configurations and their dynamics is difficult to predict.

One of the phenomena that affect electromechanical particles is the dielectrophoresis (DEP) phenomenon. The term *dielectrophoresis* describes the force exerted by a nonuniform electric field on polarizable neutral particles [1]: In a uniform electric field, neutral particles experience a polarization (an electric dipole is induced) which does not cause acceleration, whereas in a nonuniform electric field the forces due to polarization are not balanced and acceleration occurs. In particular, isolated particles experience a net force directed towards regions with either higher or lower electric field intensity, where the sign and intensity of the force depend on the polarization properties of the particle and the background medium. Pohl's first scientific publication defines DEP as "the natural movement of neutral bodies caused by polarization in an uneven electric field" [2].

Applications of DEP range from biostructure assembling [3] and nanostructure deposition (e.g., carbon nanotubes) [4] to filtering systems [5]. A branch of emerging applications is related to the controlled manipulation of micro- and nanosized particles dispersed in colloidal solutions (i.e., biological particles such as cells or DNA), since the strong selectivity of the response depends on the particle volume, shape, and composition [6]. In fact, the forces exerted by nonuniform ac electric fields, due to the frequency dependent responses, can be used to move and manipulate polarizable microparticles (such as cells, marker particles, etc.) suspended in liquid media. The DEP allows manipulation of suspended particles without direct contact: This is also significant for many applications in micro total-analysis systems (μTAS) technology [7]. Manipulation includes cell partitioning or isolation [8] for the capture or separation without the use of biomarkers: In fact, cells can be collected, concentrated, separated, and transported using the DEP forces arising from microelectrode structures having dimensions of the order of 1–100 μm [7]. One of the core strengths of DEP is therefore that the characterization of different cells depends only on the dielectric properties controlled by the particle's individual phenotype; hence, the process does not require specific tags or involve chemical reactions.

The DEP based on ac electrokinetics has recently been given more attention in microfluidics [9] due to the development of novel microfabrication techniques. In a typical

device for the capture or separation of cells, the nonuniform field for the generation of the DEP force responsible for the manipulation and control of the particles is imposed by microelectrodes patterned on substrates (typically of glass) using fabrication techniques borrowed from microelectromechanical systems (MEMS) [7]. The electric field is applied through the electrodes present in a microfluidic channel and the fluid flows through the channel.

DEP is an example of field-mediated force which, as already stated, can in principle induce a complex many-particle behavior. Therefore, predictive theoretical studies of this large class of systems could only be possible thanks to the development of real-system models and numerical simulations. Recently, particular cases and/or approximations have been considered in the literature dealing with the computational study of DEP: stable configurations of particles dispersed in a static fluid [10,11] have been determined; numerical models and simulations of the movement of cells in a moving fluid within a microfluidic channel (using the approximate DEP force calculated from commercial tools [12–14]) have been derived. Finally, exact calculations of the forces by means of commercial tools [15] in the few-particles case have been reported.

This contribution focuses on the theoretical study of the dynamics of EMPs suspended in a colloidal solution in the presence of a nonuniform variable electric field. Our numerical simulations of model systems aim at providing predictions of both stable configurations of the particles and their dynamics in fully three-dimensional configurations, minimizing the approximations usually considered in models of mutual interactions. As a case study that will be analyzed in detail, a system has been chosen consisting of biological cells dispersed in a colloidal solution (of which the typical characteristics of interest are reported in the literature) that flows into a microfluidic channel in the presence of electromagnetic fields.

Three-dimensional (3D) simulations of dielectrophoresis phenomena are rather rare in the literature, as they require large computational resources; moreover, most DEP models are based on particles in the diluted solution limit [16]. In the latter case, the DEP force is calculated using an approximate method (standard DEP). Nevertheless, in real applications, particle manipulation and characterization using dielectrophoresis are generally performed in a confined region close to the electrodes, so that the interaction between the particles and the surrounding walls can be significant. Here we run a detailed study, with a nonapproximate calculation of the forces, which are estimated by integrating the Maxwell stress tensor over the surfaces of the particles [17]. The dynamics are simulated by techniques borrowed from molecular dynamics (MD), which is a simulation method that has been successfully applied in the atomistic simulation field [18], whilst the finite element method (FEM) is applied to obtain self-consistent numerical solutions of the partial differential equations regarding the electromagnetic field. The coupled MD-FEM algorithm and its implementation in the FENICS [19] environment is also presented. The examples of the method's application will focus on DEP induced translation of spherical particles (in particular a dielectric model of MDA-MB-231 tumor cells, B-lymphocytes, and mixtures of them); however, after suitable adaptation it can be applied in more general cases (i.e., nonspherical particles, rototranslation, mixed DEP, and conventional electrophoresis).

The paper is organized as follows: In Sec. II we present the continuum formalism for the calculation of electromechanical forces, considering both the nonapproximated approach for interacting EMPs (by means of the Maxwell stress tensor based expression) and the dipole approximation valid in the diluted limit (noninteracting EMPs). In Sec. III we discuss the rest of the single-particle forces acting on the system, namely, the drag force, the lift force, and gravity. In Sec. IV we describe the numerical algorithm of our simulations. In Sec. V we describe the model of the biological layered particles. In Sec. VI we discuss a model validation for simple configurations, i.e., few particles in a parallel plate capacitor. In Sec. VII we present the model of the microfluidic channel and the MD-FEM simulation results in two many-particle systems: (a) a system composed of identical particles and (b) a system composed of two types of particles with different morphological and dielectric specifications. In Sec. VIII we present some conclusive remarks.

II. ELECTROMECHANICAL FORCES

In the formalization of our computational tool, we decided to minimize any approximation in the calculation of the field-induced forces on a particle. As a consequence the numerical evaluation of the electromagnetic forces is based on the rigorous application of the Maxwell stress tensor (MST, here and after indicated by $\overline{\overline{T}}$), and the related relationships for the evaluation of forces. Indeed, the momentum change of a volume V of a dielectric inside an electromagnetic field can be correctly expressed as a surface integral of $\overline{\overline{T}}$ [20]:

$$\frac{d}{dt}(\boldsymbol{P}_{\text{mass}} + \boldsymbol{P}_{\text{field}}) = \oint_{\Omega} \overline{\overline{T}} \cdot \hat{n} d\Omega, \tag{1}$$

where $\boldsymbol{P}_{\text{mass}}$ is the momentum of the mass contained in volume V, $\boldsymbol{P}_{\text{field}}$ is the total electromagnetic momentum of the field, Ω is the surface enclosing volume V, and $\hat{n}$ is the unit vector normal to Ω. According the electromagnetic field theory, the MST is given by the following general expression [21]:

$$\overline{\overline{T}} = \tfrac{1}{2}[\mathbf{E} \otimes \mathbf{D} + \mathbf{D} \otimes \mathbf{E} + \mathbf{B} \otimes \mathbf{H} + \mathbf{H} \otimes \mathbf{B} - (\mathbf{E} \cdot \mathbf{D} + \mathbf{B} \cdot \mathbf{H})\mathbf{I}], \tag{2}$$

where **E**- is the electric field, **D** is the electric displacement, **H**- is the magnetic field, **B** is the magnetic induction, and **I**- is the unit tensor. Products with a dot are scalar, whereas the symbol $\otimes$ indicates a dyadic tensor product of vectors. In practical dielectrophoretic applications, the applied external electromagnetic field generally has a frequency below 100 MHz and the correspondent field wave has a wavelength of the order of meters. Since the wavelength is much larger than the dimensions of typical DEP arrangements, the contribution of the magnetic field can be neglected (near field approximation). Equation (2) reads

$$\overline{\overline{T}} = \tfrac{1}{2}[\mathbf{E} \otimes \mathbf{D} + \mathbf{D} \otimes \mathbf{E} - (\mathbf{E} \cdot \mathbf{D})\mathbf{I}]. \tag{3}$$

If nonferroelectric materials compose the EMPs, a linear dependence between **D** and **E** is valid and Eq. (3)

becomes [17]

$$\overline{\overline{T}} = \mathrm{Re}\{\tilde{\varepsilon}_m\}[\mathbf{E}\otimes\mathbf{E} - \tfrac{1}{2}(\mathbf{E}\cdot\mathbf{E})\mathbf{I}], \tag{4}$$

where $\tilde{\varepsilon}_m$ is the complex permittivity of the medium. By indicating the permittivity and the electrical conductivity of the medium with ε_m and σ_m, respectively, $\tilde{\varepsilon}_m$ can be written as

$$\tilde{\varepsilon}_m = \varepsilon_m - i\frac{\sigma_m}{\omega}. \tag{5}$$

Similar to Eq. (5), the definition of the complex permittivity of the particles is

$$\tilde{\varepsilon}_p = \varepsilon_p - i\frac{\sigma_p}{\omega},$$

where ε_p and σ_p are, respectively, the permittivity and the electrical conductivity of the particle.

We assume that the motion of EMPs is induced by a harmonic nonuniform electric field and consequently we use exponential notation [20]:

$$\mathbf{E}(\mathbf{r},t) = \mathrm{Re}\{\mathbf{E}(\mathbf{r})e^{-i\omega t}\} \equiv \tfrac{1}{2}[\mathbf{E}(\mathbf{r})e^{-i\omega t} + \mathbf{E}^*(\mathbf{r})e^{i\omega t}] \tag{6}$$

By replacing Eq. (6) in Eq. (4) and by taking the time average, we obtain

$$\langle\overline{\overline{T}}\rangle = \frac{1}{2\pi}\int_0^{2\pi}\overline{\overline{T}}\,d(\omega t) = \tfrac{1}{4}\mathrm{Re}\{\tilde{\varepsilon}_m\} \times [\mathbf{E}(\mathbf{r})\otimes\mathbf{E}^*(\mathbf{r}) + \mathbf{E}^*(\mathbf{r})\otimes\mathbf{E}(\mathbf{r}) - |\mathbf{E}(\mathbf{r})|^2\,\mathbf{I}] \tag{7}$$

From Eq. (1) we see that by integrating the MST over a surface external to the particle and infinitesimally close to it, we obtain the field-induced force acting on the particle itself (as the change of the moment relative to the field is excluded). Therefore, if now we indicate with Ω this particular surface, the time-averaged electromechanical force exerted on a particle immersed in a medium with complex permittivity $\tilde{\varepsilon}_m$ and subject to sinusoidal electric field **E**- is [22]

$$\langle\boldsymbol{F}^{\mathrm{MST}}\rangle = \begin{pmatrix}\langle F_x^{\mathrm{MST}}\rangle\\ \langle F_y^{\mathrm{MST}}\rangle\\ \langle F_z^{\mathrm{MST}}\rangle\end{pmatrix} = \oint_\Omega \langle\overline{\overline{T}}\rangle\cdot\hat{n}d\Omega = \frac{1}{4}\mathrm{Re}\{\tilde{\varepsilon}_m\} \times \oint_\Omega [\mathbf{E}(\mathbf{r})\otimes\mathbf{E}^*(\mathbf{r}) + \mathbf{E}^*(\mathbf{r})\otimes\mathbf{E}(\mathbf{r}) - |\mathbf{E}(\mathbf{r})|^2\mathbf{I}]\cdot\hat{n}d\Omega. \tag{8}$$

As we can see from Eq. (8), the calculation of the electromechanical force requires the solution of the electric field, which in the case of dielectrophoretic applications derives from an applied electrical potential to electrodes. In order to evaluate the electric field, the complex Laplace equation must be solved. Again, the potential applied is time varying and harmonic:

$$\mathrm{V}(\mathbf{r},\mathrm{t}) = \mathrm{V}(\mathbf{r})e^{-i\omega t},$$

and the complex Laplace equation to be resolved is [23]

$$\nabla\cdot[\tilde{\varepsilon}\,\nabla\,\mathrm{V}(\mathbf{r})] = 0. \tag{9}$$

In Eq. (9), we must consider $\tilde{\varepsilon} = \tilde{\varepsilon}_m$ inside the liquid medium and $\tilde{\varepsilon} = \tilde{\varepsilon}_p$ inside the particles.

This equation is based on some assumptions: particle neutrality (negligible ion effect), harmonic oscillation (linear model), and negligible convection effects [24]. Moreover, as stated, the coupling of electric and magnetic fields can be neglected ($\nabla\times\mathbf{E} = -\frac{\partial\mathbf{B}}{\partial t} = 0$) and in this framework, we can derive the electric field simply as a gradient of the electrical potential:

$$\mathbf{E} = -\nabla\,\mathrm{V}(\mathbf{r}). \tag{10}$$

In the following, we will refer often to the usual approach of calculation of the dielectrophoretic force, based on the first order dipole approximation. This limit is valid in the case of particles suspended in the diluted solution, where particle-particle and particle-electrode interactions can be neglected (i.e., isolated particles). The force calculated by this approach is called "standard dielectrophoretic force". We indicate it with the symbol $\boldsymbol{F}^{\mathrm{STD}}$. For a spherical particle, the time-averaged expression of $\boldsymbol{F}^{\mathrm{STD}}$ is the following [24]:

$$\langle\boldsymbol{F}^{\mathrm{STD}}\rangle = \pi\varepsilon_m R^3\mathrm{Re}\{f_{\mathrm{CM}}\}\nabla(|\mathbf{E}|^2) = 2\pi\varepsilon_m R^3\mathrm{Re}\{f_{\mathrm{CM}}\}\nabla(|\mathbf{E}_{\mathrm{rms}}|^2), \tag{11}$$

where $f_{\mathrm{CM}} = \frac{\tilde{\varepsilon}_p - \tilde{\varepsilon}_m}{\tilde{\varepsilon}_p + 2\tilde{\varepsilon}_m}$ is the Clausius-Mossotti factor, R is the particle radius, and $\mathbf{E}_{\mathrm{rms}}$ is the root mean square of the electric field. The strength of $\langle\boldsymbol{F}^{\mathrm{STD}}\rangle$ depends on the dielectric properties of the particle and medium, the shape and size of the particle, and the intensity and frequency of the oscillating electric field. The angular frequency influences the complex permittivity of the particle and the medium, which in turn affect the Clausius-Mossotti factor, and therefore the force. Indeed, $\mathrm{Re}[f_{\mathrm{CM}}]$ determines both the magnitude and the sign of the DEP force. Consequently, due to its characteristics, the DEP force allows the control of particles of micrometric size dispersed in colloidal solutions. In sorting operation mode, when two types of particles are present, the frequency can be chosen for the capturing and separations, so one particle type experiences negative DEP (n-DEP, $\mathrm{Re}\{f_{\mathrm{CM}}\} < 0$) moving away from the electrodes, and the second type experiences positive-DEP (p-DEP, $\mathrm{Re}\{f_{\mathrm{CM}}\} > 0$), moving towards the electrodes, as seen in Eq. (11).

In the systems based on diluted solutions (i.e., almost isolated particles), the first order dipole approximation [Eq. (11)] is reasonable. However, particle manipulation and characterization using DEP is generally performed in a confined region close to the electrodes where particles accumulate. Moreover, in the modeling of biological cells, among others, their typical dimensions are often comparable to the electrode ones. For these reasons, an accurate approach for calculating the DEP forces is necessary. The use of $\langle\boldsymbol{F}^{\mathrm{MST}}\rangle$, instead of $\langle\boldsymbol{F}^{\mathrm{STD}}\rangle$ allows the correct description in the proximity of the electrodes when the particle-particle electromechanical interactions cannot be neglected due to the relatively large local density of EMPs.

We note that improvements with respect to the standard DEP theory based on $\langle\boldsymbol{F}^{\mathrm{STD}}\rangle$ could be obtained considering dipole-dipole interactions [10,11,15]. These approximated "two-body" interactions reproduce qualitatively part of the EMP behavior [11,15] and schematize their interactions. Anyhow, this approximation could be strongly inaccurate in the general case, since the electromechanical interactions are in general "many-body" forces which in the near field (i.e., when the particles are close to each other and close to the external source of the field, e.g., the electrodes) deviate from the dipole-dipole ones. For example, in Ref. [15] the simple case

of a single spherical particle close to a planar electrode was studied; even in this simple configuration the Maxwell tensor calculation of the forces is significantly different from the dipole-dipole estimate. Of course, these deviations become stronger for systems that are more complex (e.g., for many particles close to each other and/or close to the electrodes). Moreover, electromagnetic interactions in general depend also on the shape of the particles and electrodes, and a generic analytical formulation is difficult even when considering a multipole expansion. In the following, we demonstrate that the use of the Maxwell stress tensor makes feasible the implementation in a FEM framework, which can be extended in the generic case without the need of "ad hoc" formulations.

III. SINGLE PARTICLE EXTERNAL INTERACTIONS

For realistic simulations, other forces must also be taken into account in addition to the electromechanical forces. EMPs in manipulation experiments are not only subjected to electromagnetic fields, but also to hydrodynamic pressure fields and to gravity. Consequently, in order to apply the proposed MD-FEM approach to relevant cases of study, we assume that particles are also subjected to interactions describing additional effects occurring in colloidal solution. In experimental systems, a controlled hydrodynamics is implemented where both fluid-wall and particle-fluid interactions are well within the laminar regime [25].

In these conditions, these external interactions act on "single particles" and for spherical ones can be expressed as analytical expressions of their kinetic variables. We note that in general we will consider that the colloidal solution containing the EMPs is not static, although some case studies will be discussed in the limit of static solutions. The viscous drag force stemming from the viscosity of the medium is given for a spherical object by [26]

$$\boldsymbol{F}_{\text{drag}} = 6\pi\mu R(\boldsymbol{u} - \boldsymbol{v}), \tag{12}$$

where μ is the dynamic viscosity, $\boldsymbol{u}$ is the local velocity of the fluid, and $\boldsymbol{v}$ is the instantaneous velocity of the particle.

The lift force, due to the non-negligible velocity gradient of the fluid across the particle surface, is also present [27] and it is particularly important close to the sidewalls of the channel containing the solution. In the application of our MD-FEM method, we will consider a microfluidic channel with parallel sidewalls and small dimensions, where the fluid flow can be assumed laminar since the Reynolds number relative to the channel is about 0.006 while that relative to the spherical particles is of the order of 10^{-6}. In these conditions, by neglecting any disturbance due to the particles' presence on the velocity fluid field, the shape of the flow profile in the vertical direction of the channel depends parametrically only on the chamber height h. The analytical solution of the fluid velocity field is the parabolic flow profile [28]:

$$u(z) = 4u_{\max}\,\frac{z}{h}\,\frac{h-z}{h},$$

where z is the distance of the particle center from the bottom of the channel and $u_{\max} = u(\frac{h}{2})$ is the velocity of the fluid at the center of the channel, as shown in Fig. 1. We note that $u(0) = u(h) = 0$. The lift force arises because of the fluid

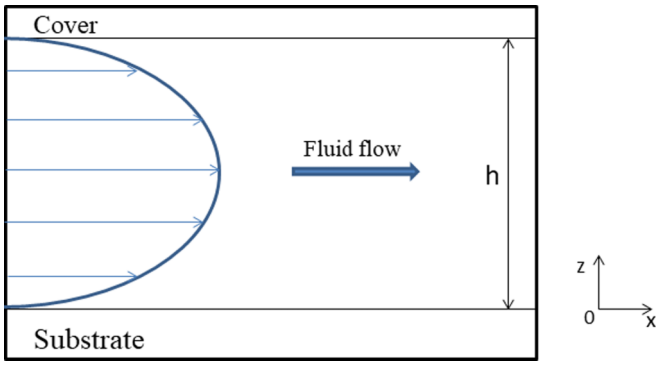

FIG. 1. Parabolic velocity profile for a fluid flowing through a microfluidic channel of height h; $u(0) = u(h) = 0$; $u_{\max} = u(\frac{h}{2})$.

viscous flow on particles close to a solid plane, causing their levitation [29] and, in this particular channel geometry, it is perpendicular to the bottom and directed towards the center of the channel. Its intensity is directly proportional to the gradient of the curve describing the fluid velocity [Eq. (12)] and it takes the following form [30]:

$$F_{\text{lift}} = \frac{C\mu R^3}{(z-R)}\,\frac{d}{dz}u(z)\bigg|_{z=0} = \frac{4C\mu R^3 u_{\max}}{h(z-R)}, \tag{13}$$

where $C = 0.153$.

The summation of gravitational force acting on spherical cells and the buoyancy force (due to the density of the surrounding fluid and the amount of fluid displaced by the particles) is

$$\boldsymbol{F}_{\boldsymbol{g}} = \tfrac{4}{3}\pi R^3(\rho_p - \rho_m)\mathbf{g}, \tag{14}$$

where ρ_p and ρ_m are the particle and suspension medium density, respectively, and $\mathbf{g}$- is the acceleration due to gravity.

Summarizing, from the considerations of this section we can conclude that the forces acting on the particles are as follows:

along the x axis: $\langle F_x^{\text{MST}}\rangle$ and viscous drag force;

along the y axis: $\langle F_y^{\text{MST}}\rangle$ and viscous drag force;

along the z axis: $\langle F_z^{\text{MST}}\rangle$, viscous drag force, lift force, gravity, and buoyancy force.

We notice that the different degrees of accuracy between the hydrodynamic and electromagnetic interactions, considered in our computational approach, are justified by the fact that the latter dominate the particle dynamics, at least for the examples considered in our analysis. The reliability of the expressions (12) and (13) will be quantitatively discussed in Sec. VII, where simulation results of realistic systems will be presented. Although beyond the scope of the present paper, the MD-FEM strategy can also be applied to other fluidic regimes considering different expressions for the single particle interactions [Eqs. (12)–(14)] or extending the FEM solutions to the Navier-Stokes equations with an appropriate numerical evaluation of the fluid kinetics and the pressure forces on the particles.

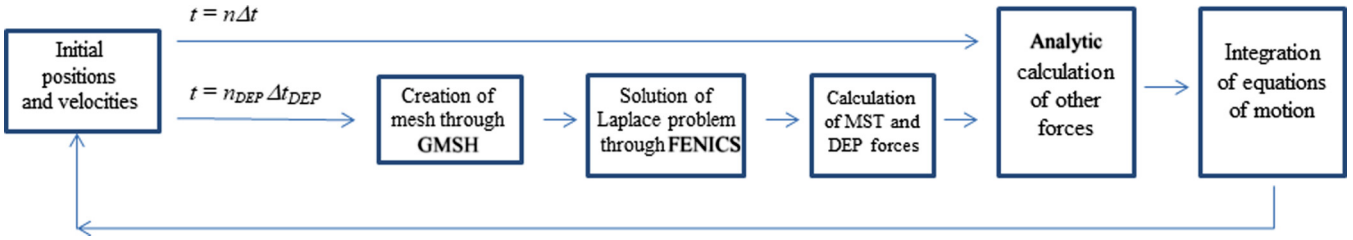

FIG. 2. Block diagram of the MD-FEM algorithm. n and n_{DEP} are integers greater than or equal to zero, such that $n/n_{\mathrm{DEP}} = \Delta t_{\mathrm{DEP}}/\Delta t$.

IV. NUMERICAL ALGORITHM

Our code, distributed as open source (see Ref. [31]) aims at evaluating the evolution of a system of EMPs by using MD techniques for the integration of the equations of motion. The simulation of the particle kinetics then consists of a sequence of loops with the following steps: system configuration preparation from the known positions and velocities of the particles; calculation of forces acting on the particles and then of the corresponding accelerations; integration of the equations of motion for a suitable time increment; new configuration setting. The calculation of the electromechanical force [Eq. (8)] acting on the particles needs the solution of the Laplace problem with a complex potential variable in a 3D geometry; i.e., the partial differential equation (PDE) needs to be solved in a numerical domain reproducing the system configuration. Other forces are instead calculated analytically by means of Eqs. (12)–(14).

The complex Laplace equation is solved using a finite element method. In particular, we integrate in our code the PYTHON methods of FENICS [19], an open source software package that offers a complete platform for solving PDEs with the use of FEM. For the 3D computational mesh generation relative to the system configuration our code instead integrates GMSH [32], which is an open-source computer-aided engineering platform which operates on the basis of parametric inputs. This allows the interaction between the FEM part and the MD part of our code. Finally, the particlelike molecular-dynamics technique extracts the forces from the FEM continuum solution in the so-called coupled MD-FEM technique. We analyze in detail each step of the simulation in the following.

Computational domain. Figure 2 shows the procedure to simulate the system evolution. We consider a number of particles with their initial position and velocities, at the instant t_0. The first step of the simulations is to create, through the functionality of GMSH, the mesh relative to the spheres (which represent the particles) embedded in the box (which represents the microfluidic channel) also including the electrode geometries. All these portions of the numerical domain are merged in a single mesh, but it is necessary to identify and label them in a univocal way. Note that the dimensions of the particles and simulation box entities as well as the local resolution of the mesh in the different geometric elements can be defined independently.

FEM solutions and forces' estimates. The second step is the solution of the Laplace problem, which is a prerogative of FENICS. Dirichlet boundary conditions for the applied potentials on the electrodes and on the microchannel top surface are used, whereas Neumann boundary conditions are used for most other exterior boundaries to model their electrical insulation. Eventual periodic boundary conditions can also be activated if necessary. Using the FEM solution (i.e., the distribution of the complex potential in space), we also calculate by applying some FENICS functionalities: the values of the electric field, the Maxwell stress tensor by Eq. (7), and finally the electromechanical force by Eq. (8). After this computationally intensive part, the single particle interactions are calculated from the analytic expressions reported in the previous section, which depend on the velocity field of the fluid.

Integration of the equations of motion. We calculate the accelerations of the particles from the resulting forces and proceed with the numerical integration of the equations of motion by means of the Verlet velocity method technique [33], which consists of the following procedure. At a given time step t, for the particle occupying position $\boldsymbol{r}$ and having initial velocity $\boldsymbol{v}$, the updated position and velocity in the next time step $t + \Delta t$ are evaluated as follows [34]:

$$\text{calculate}\quad \boldsymbol{r}(t+\Delta t) = \boldsymbol{r}(t) + \boldsymbol{v}(t)\Delta t + \tfrac{1}{2}\boldsymbol{a}(t)\Delta t^2, \tag{15}$$

$$\text{derive}\quad \boldsymbol{a}(t+\Delta t)\ \text{ using }\ \boldsymbol{r}(t+\Delta t), \tag{16}$$

$$\text{calculate}\quad \boldsymbol{v}(t+\Delta t) = \boldsymbol{v}(t) + \frac{\boldsymbol{a}(t)+\boldsymbol{a}(t+\Delta t)}{2}\Delta t, \tag{17}$$

where the time increment Δt rules the time accuracy of the method. A slight modification of the conventional Verlet algorithm is considered, since the acceleration contains a velocity dependent term that can be explicitly evaluated in the finite difference Eq. (17). Random Brownian forces, relevant for very small (nanometric) EMPs, are neglected; however, they can be considered in future extensions implementing the Brünger-Brooks-Karplus (BBK) algorithm for the Langevin dynamics [35].

Our MD step includes control instructions on steric particle-particle and particle-wall interactions, which can be also considered as particular hard-sphere-like particle-particle interactions [36]. Indeed, particles must never exceed the walls of the simulation box in their dynamics; moreover, particles must not penetrate each other. For each MD step, checks are carried out: If one or both of these events occur, one check modifies the velocities and positions of the particles as explained below. The interaction between the particles and the walls is conceived in terms of an elastic impact: If a particle is found to have crossed the wall of the box in an MD step, its center is associated with a new value of speed

(the opposite vector with respect to the one it had) and with the position occupied before crossing the wall. In the case of overlapping between particles, they are separated from each other, along the center-center direction, by a minimum distance so that they do not penetrate each other. Unlike in the case of particle-wall interaction, the check in this case does not change the particle speeds but only their positions; in other words, the problem is not treated in terms of elastic impact. This procedure is motivated by the presence of the drag force [Eq. (11)] which depends on the speed. It is assumed that the drag force strongly influences the particle-particle interaction modifying immediately the effects of the elastic impact. Such procedures avoid nonphysical situations, which, among other things, lead to conflicts in the generation of the mesh of the box and subdomains at the FEM computational phase.

We note that for future applications of our code in more critical hydrodynamic regimes than the one discussed previously, the control loop for the steric interactions could be generalized in order to include analytic expressions of hydrodynamic nature for the particle-particle and particle-wall effective interactions (see, e.g., Chaps. 6 and 7 of Ref. [37] or Part III, Chaps. 7–13 of Ref. [38]). This approach could be alternative to the FEM numerical solutions of the Navier-Stokes equations, which in turn might not be computationally feasible in our coupled scheme.

It is evident that the MD-FEM coupling implies considerable computational resources, since the result obtained in a calculation cycle constitutes the initial condition of a further cycle relative to the following time step, and both remeshing and FEM procedures have to be performed at each iteration cycle. As a consequence, to satisfy both accuracy and efficiency requirements, we have dynamically adapted [33] the optimal MD time step in order to maintain the module of the difference between the forces acting on the particles between two successive steps below 200 pN. This threshold is comparable with the ones made in the usual MD approaches considering the different inertia of the particles (atoms vs cell). Moreover, in order to optimize further the simulation time, we decouple the calculation of the electromagnetic force from the analytical calculation of other forces (which is significantly faster). Indeed, we note that electromagnetic forces usually show appreciable variations on time scales larger with respect to the cited optimal values of the MD increment Δt, which in turn is maximally ruled by the other forces (especially drag and steric interactions). Consequently, we introduce two time steps: Δt, already seen in Eqs. (15)–(17) in relation to the velocity Verlet algorithm, which optimizes the calculation of the drag and lift forces and of steric interactions, and Δt_{DEP}, i.e., the time interval between one remeshing and FEM calculation and the subsequent one. The first type of cycle is performed for $t = n\Delta t$ while the second type is performed for $t = n_{\mathrm{DEP}}\Delta t_{\mathrm{DEP}}$, where n and n_{DEP} are integers greater than or equal to zero, such that $n/n_{\mathrm{DEP}} = \Delta t_{\mathrm{DEP}}/\Delta t$. This decoupled method is clearly more efficient. Figure 2 shows a block diagram of this MD-FEM algorithm.

V. PARTICLE MODEL

It is clear from Eq. (9) that it is necessary to know the complex dielectric constant of the particle at the operational frequency ω for calculating the dielectrophoretic force. In the application example of the MD-FEM method we consider biological cells; therefore a derivation of the dielectric parameter for such particular system is necessary. The expression first introduced by Pohl is based on modeling the cell as a solid spherical dielectric particle suspended in a fluid medium. Circulating tumor cells are often modeled as rigid spheres [39]. However, biological particles are complex and heterogeneous structures with multiple layers having distinct electrical properties [40]. In biological dielectrophoresis, it is thus essential to adopt trusted dielectric models for such particles. A more realistic model for cells has been adopted in this work: The cell is represented by a spherical dielectric core and a spherical dielectric shell to account specifically for the dielectric properties (conductivity and permittivity) of the cytoplasm and of the plasma membrane, respectively. We apply the "effective electrical permittivity" $\tilde{\varepsilon}_{\mathrm{eff}}$ method, taking into account the properties of the different parts of the cell [7]. Consider the concentric, dielectric shelled model in Fig. 3(a), where d is the membrane thickness, R is the radius of the cell, and R–d is the difference of the cytoplasm radius.

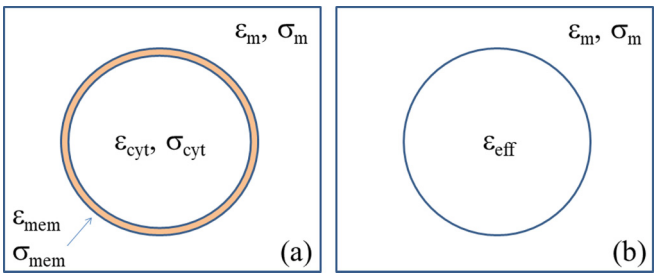

FIG. 3. (a): Spherical dielectric cell composed of the cytoplasm (inner volume) and the membrane (light brown shell indicated by the arrow). (b) Effective equivalent homogeneous sphere model ruled by the dielectric function $\tilde{\varepsilon}_{\mathrm{eff}}$.

If the conductivity of the cytoplasm and of the membrane are σ_{cyt} and σ_{mem}, respectively, the complex permittivity of the cytoplasm is $\tilde{\varepsilon}_{\mathrm{cyt}} = \varepsilon_{\mathrm{cyt}} - i\sigma_{\mathrm{cyt}}/\omega$ and the complex permittivity of the membrane is $\tilde{\varepsilon}_{\mathrm{mem}} = \varepsilon_{\mathrm{mem}} - i\sigma_{\mathrm{mem}}/\omega$. It can be shown that the induced electrostatic potential outside the particle, that is, for $|r| > R$, is indistinguishable from that of the equivalent, homogeneous dielectric sphere of radius R with permittivity $\tilde{\varepsilon}_{\mathrm{eff}}$ as shown in Fig. 3(b) [1]. The particle is thus replaced by an equivalent and homogeneous sphere with a radius equal to that of the outermost shell but with different dielectric characteristics. The complex dielectric constant $\tilde{\varepsilon}_{\mathrm{eff}}$ can be approximated by the following equation [41]:

$$\tilde{\varepsilon}_{\mathrm{eff}} = \tilde{\varepsilon}_{\mathrm{mem}} \frac{\left(\frac{R}{R-d}\right)^3 + 2\,\frac{\tilde{\varepsilon}_{\mathrm{cyt}} - \tilde{\varepsilon}_{\mathrm{mem}}}{\tilde{\varepsilon}_{\mathrm{cyt}} + 2\tilde{\varepsilon}_{\mathrm{mem}}}}{\left(\frac{R}{R-d}\right)^3 - \frac{\tilde{\varepsilon}_{\mathrm{cyt}} - \tilde{\varepsilon}_{\mathrm{mem}}}{\tilde{\varepsilon}_{\mathrm{cyt}} + 2\tilde{\varepsilon}_{\mathrm{mem}}}}.$$

In the final analysis, the quantity $\tilde{\varepsilon}_p$ present in the equations of the preceding paragraphs must be replaced by $\tilde{\varepsilon}_{\mathrm{eff}}$.

VI. MODEL VALIDATION FOR SIMPLE CONFIGURATIONS

The simulations we present in this section concern a simple device configuration to validate our numerical approach based

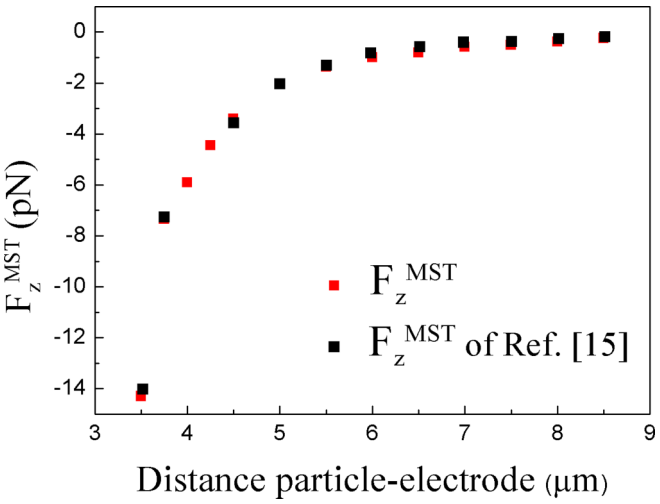

FIG. 4. Comparison between the values of F^{MST} present in Ref. [15], obtained by COMSOL, and the values calculated in our GMSH-FENICS implementation of the electromechanical force calculation.

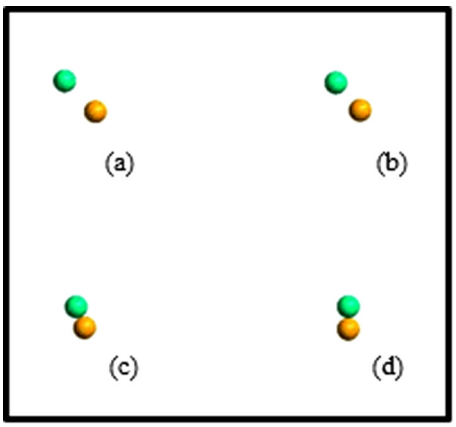

FIG. 5. Snapshots of simulation of two particles in a parallel plate capacitor for $t = 0,\ 0.1,\ 0.15,\ 0.21$ s [(a)–(d), respectively]. The particles attract and form a chain that aligns with the electric field and remains in this stable configuration for the rest of the simulated evolution.

on the MD-FEM technique: i.e., the parallel plate capacitor. The electric field is generated by the two parallel electrodes separated by a distance h. The only component of the electric field different from zero is that along the direction perpendicular to the plates, and its value in the module is

$$E = V/h,$$

where V is the electric potential drop across the plates. The first system we consider is a single particle immersed in a fluid present inside the capacitor. We use for this particle the following electrical parameters (representative of the B-lymphocytes cell, which has been well characterized [42,43]): $\varepsilon_{\mathrm{mem}} = 14.26\ \varepsilon_0$, $\sigma_{\mathrm{mem}} = 1\ \mu$S/m, $\varepsilon_{\mathrm{cyt}} = 59\ \varepsilon_0$, $\sigma_{\mathrm{cyt}} = 0.31$ S/m; its geometrical properties are as follows: $R = 3.3\,\mu$m is the radius of the cell; $d = 10$ nm is the thickness of the membrane. The values relative to the medium fluid are $\varepsilon_m = 79\varepsilon_0$, $\sigma_m = 0.03$ S/m (these values are typical for isotonic water solutions). In the calculation, the drop of potential between the plates of the capacitor is $V = 10$ V, $h = 500\ \mu$m, while the frequency of the electric field is $\nu = 1$ MHz (the angular frequency is $\omega = 2\pi\nu$).

The DEP force values calculated by the approximate formula of Eq. (11) are equal to zero as the electric field is constant inside the capacitor. The force calculated by MST has, instead, values different from zero due to the alteration induced to the total electric field by the particle in the electrode proximity (see Ref. [15] for a complete discussion).

We compare our results with those of Ref. [15] to validate our approach. In this reference the calculations are made by COMSOL MULTIPHYSICS [44], which is a commercial solver and simulation software based on finite element analysis. We note that in COMSOL it is possible to use the function "dielectrophoretic force" present in its functions library. Figure 4 shows the comparison between the values of F^{MST} for several particle-electrode distance values present in Ref. [15] and our analogous values. The value of F^{MST} is stronger close to the plate and becomes less intense as it moves away.

Our results are very similar to the ones obtained by COMSOL in Ref. [15], whereas small differences are due to the different meshes and numerical integration schemes employed.

The second check of our code is done considering two particles (B-lymphocytes) in a capacitorlike configuration of the device similar to that of the previous case. In the presence of an electric field, the formation of chains of particles is predicted [45]. It consists in the end-to-end attachment of particles, which assume a formation similar to that of a chain of pearls. The formation of particle chains is a phenomenon mainly due to the electrostatic interactions among the particles under the effects of the electric field. It occurs because the particles acquire induced dipole moments under the field action: If two particles are close to each other, the positive charge of the dipole of the first particle interacts with the negative charge of the dipole of the second; hence, they experience an attractive force which links them together. Pearl chains are formed only when the particles come close to each other and this phenomenon can be neglected in the dilute solution limit, when the particles are separated by large distances. As for elongated single particles (including biological cells), a frequency dependent orientation effect is expected for chains of homogeneous conducting dielectric spheres suspended in fluids and subjected to an electric field [46]: Chains are predicted to align with the vector joining the centers parallel to the field direction. The formation of chains is a common occurrence in DEP experiments on biological cells. In our analysis, we consider the kinetics of chain formation for lymphocytes.

The drop of potential between the plates of the capacitor is $V = 10$ V; $h = 100\ \mu$m. The frequency of the electric field is $\nu = 1$ MHz. Figure 5(a) shows the particles in the initial configuration, at time $t = 0$ s. Figures 5(b)–5(d) show the particles in successive instants, after application of a uniform electric field directed along the z axis. We note that a chain forms, due to the polarization of the particles, and also aligns itself with the electric field as time passes.

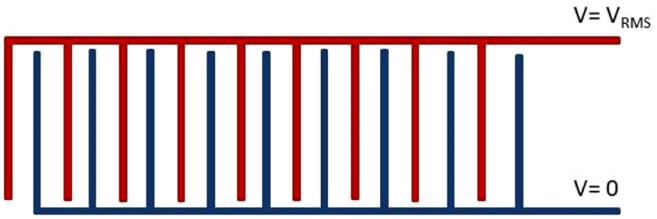

FIG. 6. Schematic of an interdigitated circuit. An alternating signal is applied to the electrodes in red while $V = 0$ is imposed to electrodes in blue.

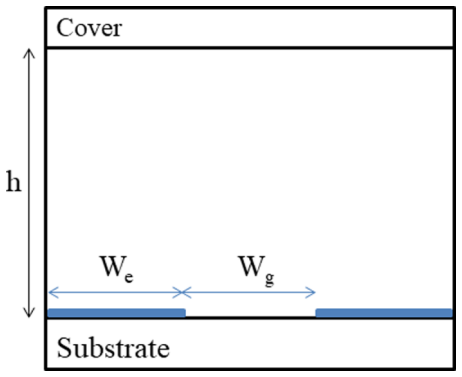

FIG. 7. Schematic of the computational domain (limited for simplicity to only two electrodes while in the simulation N electrodes are considered). The electrodes (in blue) have a width W_e and are separated by a gap of width W_g.

VII. MD-FEM SIMULATION RESULTS IN MANY-PARTICLE SYSTEMS

In this section, we discuss some results of the application of our MD-FEM method to many-particle systems which reproduce the condition of real manipulation experiments where DEP forces are induced on cells. The nonuniform electric field used in DEP applications is typically produced by electrodes with feature size in the scale of microns in order to suitably reduce the value of the applied voltage [47]. Several electrode geometries have been developed according to the particular application scopes. Lithography techniques are typically used to pattern planar electrodes on the bottom of the microchannel and examples of planar electrode designs include interdigitated [48], castellated [49], spiral [50], curved [51], oblique [52], quadrupole [53], matrix [54], and polynomial [55] electrodes.

In particular, the prototype devices for cell capture or separation have planar electrodes. The devices are composed of the following parts: a microfluidic channel (where the colloidal solution flows) and electrodes made with a geometry such as to generate a nonuniform electric field when they are subjected to an alternating electric signal.

In order to apply our method to a particular application example, the geometry used in our work is the interdigitated circuit (shown in Fig. 6) which is assumed to be incorporated in one boundary of the microfluidic channel.

An alternating signal is applied to the odd-position electrodes (shown in red in Fig. 6), while the even-position electrodes (blue in Fig. 6) are potential free ($V = 0$). The simulated system consists of cells in colloidal solution in a liquid medium that flows through the microfluidic channel. The channel is represented in the simulations by a box (parallelepiped), and in its base we identify the surface mesh region in which the electrical signal is applied.

It is necessary to make some assumptions to perform the simulations [56]: (a) Each individual "finger" comprising the interdigitated electrode array is sufficiently long such that the fringe effect at the end of the fingers is negligible. (b) Ohmic heating due to the applied voltage is not large enough to cause flows or changes in the physical constants (an approximate calculation shows that the temperature rise for this type of application will be less than 0.15 °C; consequently, this is a valid assumption [57]).

The microfluidic chamber is simulated according to these assumptions. The channel is composed of N electrodes. The electrode thickness was ignored. Figure 7 shows a schematic representation of the geometry of our simulations, which includes the substrate, channel cover, and two fingers of interdigitated electrodes. W_e is the width of the electrodes, W_g is the width of the gap between a pair of electrodes, and h is the height of the microchannel.

We present below the results of simulations of the dynamics of the system composed by a colloidal solution of cells in the microfluidic system with interdigitated electrodes. We performed two types of simulations: (a) twenty MDA-MB-231 cells under p-DEP conditions and (b) ten MDA-MB-231 cells and ten B-lymphocytes, in p-DEP and n-DEP, respectively.

In the case of simulation (a), we used the following electrical parameters representative of MDA-231 cells [58]: $\varepsilon_{\text{mem}} = 24\ \varepsilon_0$, $\sigma_{\text{mem}} = 1 \times\ 10^{-7}\ \mu\text{S/m}$, $\varepsilon_{\text{cyt}} = 50\varepsilon_0$, $\sigma_{\text{cyt}} = 0.2\ \text{S/m}$. The mass of an MDA-MB-231 cell is $m = 1.05 \times 10^{-12}\ \text{kg}$; its radius is $R = 6.2\ \mu\text{m}$; $d = 10\ \text{nm}$ is the thickness of the membrane. We used the following values for the fluid medium: $\varepsilon_m = 79\varepsilon_0$, $\sigma_m = 0.03\ \text{S/m}$, $u_{\max} = 100\ \mu\text{m/s}$. The frequency of the electric field was $\nu = 1$ MHz. The dimensions of the microchannel were $(960 \times 60 \times 100)\ \mu\text{m}^3$ (for the length, depth, and height, respectively). The width of the electrodes was $W_e = 40\ \mu\text{m}$, the gap between them was $W_g = 40\ \mu\text{m}$, and their number was 12. The time steps, calibrated in order to ensure stability and time accuracy to the explicit MD integration method, were $\Delta t = 3 \times 10^{-5}\ \text{s}$, $\Delta t_{\text{DEP}} = 6 \times 10^{-4}\ \text{s}$.

The electromagnetic force varies as a function of the magnitude and frequency of the input voltage and a high voltage should be applied to generate intense DEP forces, but excessive loading can cause cell damage (harm cell viability) orelectrothermal flows [14]. For these reasons, a trade-off between DEP intensity and safe conditions for the biological system was considered in the experimental conditions, and usually voltages less than 10 V_{p-p} were applied. In our simulation, the potential $V = 5\,\text{V}$ was applied to the set of odd electrodes, whereas $V = 0\,\text{V}$ was applied to the set of even ones. The boundary conditions, in addition to the predefined voltages on the electrode surfaces, consist of insulation (Neumann-type boundary condition) on the channel walls, because of the large difference between the permittivities and the conductivities of the liquid medium and the channel material, which is either glass or polymer based in the majority

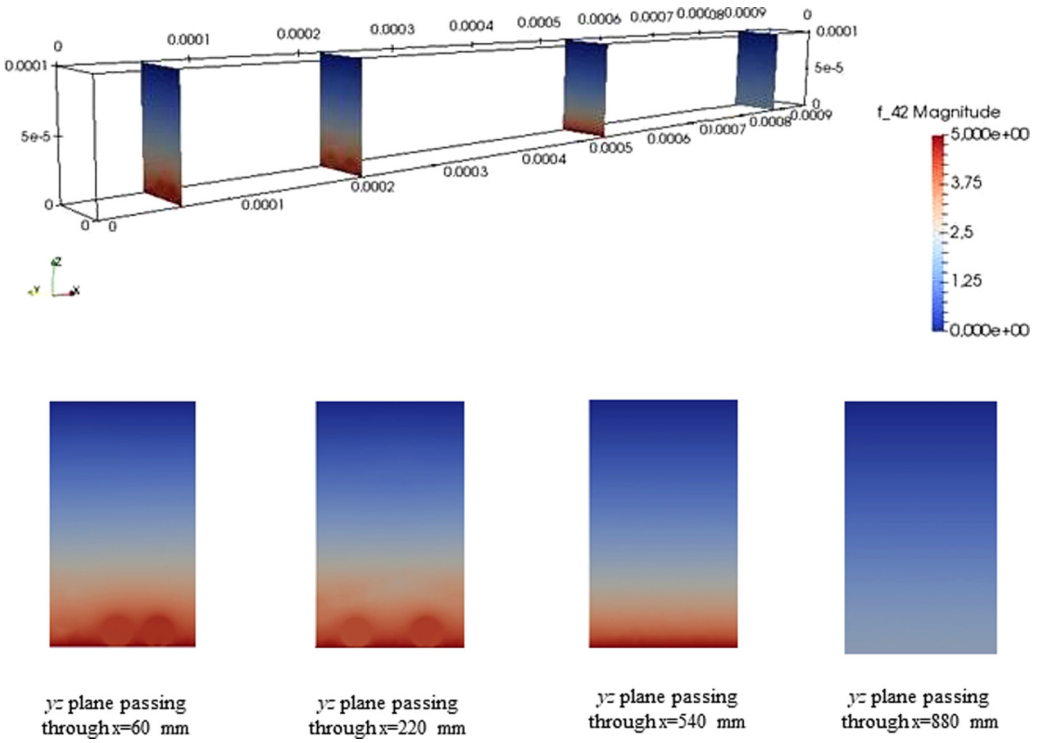

FIG. 8. Solution of the Laplace problem at $t = 0.6$ s. Top panel: the schematic of the microfluidic channel in which the solution of the Laplace equation relative to the sections passing through $x = 60,\ 220,\ 540$, and 880 μm is visible. Bottom panel: the front views of the slices themselves, where variations in potential due to the presence of particles can be observed.

of the cases. Neumann-type boundary conditions were also applied in the surface regions of the microchannel base that were not covered by electrodes. As an initial condition, the particles were arranged in a configuration characterized by random positions, concentrated in the left side of the channel, corresponding to about one-third of the total volume (i.e., a local injection of particles was reproduced).

During the simulation, the self-consistent FEM solutions of Eq. (9) were calculated considering the instantaneous configuration of the system. In Fig. 8 we show the solution of the time harmonic Laplace problem at $t = 0.6$ s (as an example), relative to four sections of the microfluidic channel: the first crosses the channel in the $x = 60\,\mu$m plane, the second in $x = 220\,\mu$m, the third in $x = 540\,\mu$m, and the fourth in $x = 880\,\mu$m. In this instant, some particles are located at the edges of the electrode centered in $x = 40\,\mu$m and of the second centered in $x = 200\,\mu$m. The perturbations to the potential generated by the external field due to the particle presence (and corresponding polarization) can be seen in the sections.

As can be deduced from Fig. 8, the gradient of the electric field is more intense in the areas close to the base of the microfluidic channel, and in particular in the regions close to the edges of the electrodes. As a result, forces are more intense in these areas. In the snapshots of planes passing through $x = 60\,\mu$m and $x = 220\,\mu$m, it is possible to clearly identify the effects on the electrical potential due to the presence of particles occupying the regions close to the edges of the two electrodes.

Figure 9 shows snapshots of the simulation results at several instances of time, from $t = 0$ s to $t = 5.1$ s (different colors are used to identify the cells but, of course, they are identical in terms of dielectric properties).

The simulations carried out on this system show, as expected, that the particles undergo attractive forces from the zones in which the gradient of the electric field is greater. In particular, they are attracted by the edge of the electrode. The particles, which have a smaller distance from the electrode, are attracted more strongly since the gradient is greater in these regions. In the topmost part of the channel, the field is more uniform, so that particles in this region of the device will be subjected to less intense attractive forces and they continue to advance with minor height reduction. When their altitude with respect to the channel base is sufficiently small and they reach zones where the nonuniformity of the field is greater, the attraction becomes stronger and the trapping effect becomes evident. Particles that reach the base of the device and thicken close to the edges of the electrodes have small variations of their position as a result of the various forces acting on them; anyway it is correct to say that they remain trapped in these regions.

An additional behavior that can be observed, in the case of spatial proximity between particles, is the chain formation in dynamical conditions caused by mutual polarization. Figure 10 shows a more detailed analysis of the behavior of a pair of particles that attract each other and form a pair (chain), which moves as a single object and is attracted by the edge of an electrode. The pair is circled in the first snapshot of Fig. 10. It is possible to note that after the pair formation in the time evolution the two particles present a cohesive motion until they reach the bottom, whose influence could, of course, overcome particle-particle interactions.

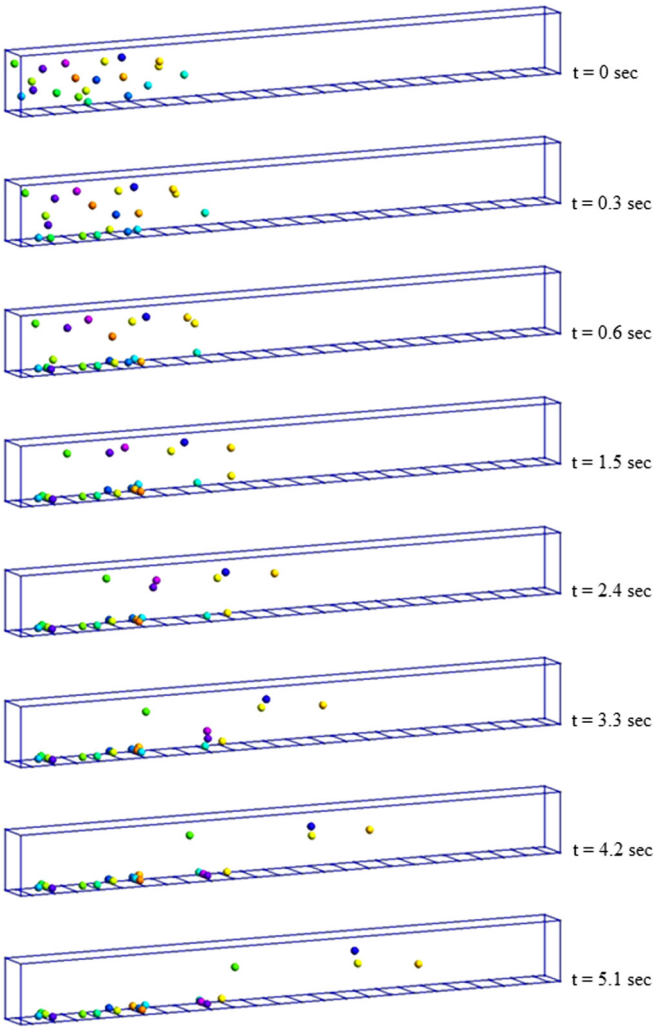

FIG. 9. Snapshots of simulated system ($N = 20$ MDA-MD-231 cells in a flowing colloidal solution) for $t = 0,\ 0.3,\ 0.6,\ 1.5,\ 2.4,\ 3.3,\ 4.2,\ 5.1$ s (from upper panel to lower panel). The dimensions of the microchannel are $(960\ \times 60 \times\ 100)\,\mu\text{m}^3$ (for the length, depth, and height, respectively) and the number of electrodes is 12.

With respect to simulation (b) (ten cells of MDA-MB-231 and ten B-lymphocytes), the morphological and electrical characteristics of both cell types have already been listed in this work. The width of the electrodes and the distance between them are the same as that of the previous simulation, but the number of electrodes this time is $N = 10$ and thus the dimensions of the microchannel are $(800 \times 60 \times 100)\,\mu\text{m}^3$ (for the length, depth, and height, respectively).

A relevant parameter that has been modified with respect to the previous study of 20 identical particles is the oscillation frequency of the electric field: In this second simulation, it has been set to $\nu = 10^5$ Hz. An anticipation of the behavior of the two types of cells, in the diluted solution limit, for this frequency value can be given by the real part of the Clausius-Mossotti factor, which has the following values for the two types:

MDA-MB-231: $\text{Re}\{f_{\text{CM}}\} = 0.378$,

B-lymphocytes: $\text{Re}\{f_{\text{CM}}\} = -0.22$.

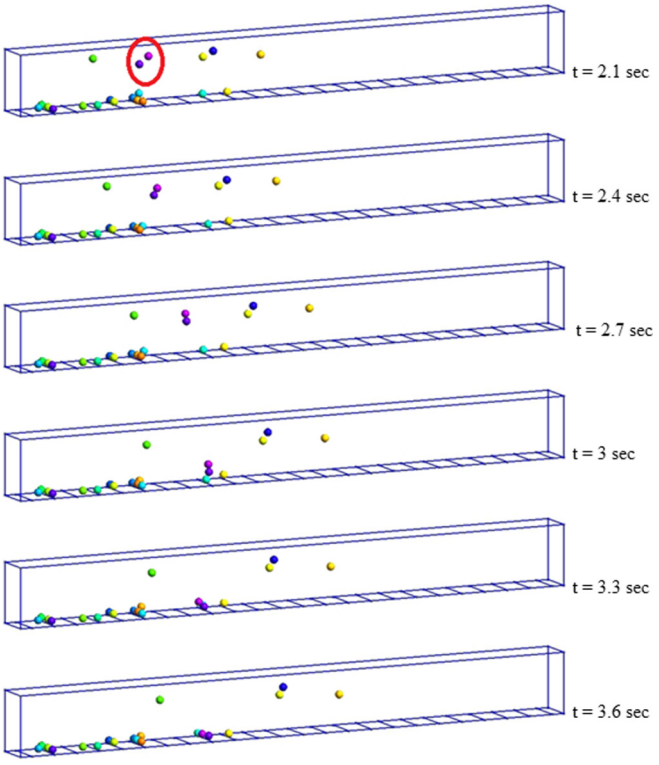

FIG. 10. Snapshots for $t = 2.1,\ 2.4,\ 2.7,\ 3,\ 3.3,\ 3.6$ s (from upper to lower). The pair of particles that form the chain is circled in the upper snapshot. The dimensions of the microchannel are $(960\ \times\ 60\ \times 100)\,\mu\text{m}^3$ (for the length, depth, and height, respectively) and the number of electrodes is 12.

These values refer to the calculation of the standard DEP force in the approximation of isolated particles on an infinite medium, but can nevertheless provide a guideline in most realistic cases that we analyze with the simulation. For this frequency value, the two values of $\text{Re}\{f_{\text{CM}}\}$ indicate that MDA-MB-231 cells are subject to p-DEP and are attracted to areas where the electrical field gradient is higher (that is, from the regions near the electrodes and especially from their edges), while B-lymphocytes are subject to n-DEP and are rejected from these regions. Figure 11 shows the simulation results at several instances of time, from $t = 0$ s to $t = 5.1$ s.

The simulation qualitatively follows the behavior predicted for the two values of $\text{Re}\{f_{\text{CM}}\}$. The MDA-MB-231 cells are attracted to the electrodes as in the case of simulation (a), while B-lymphocytes are rejected and do not reach the base of the device. This behavior confirms the separation or capture potential of this type of electrophoretic device. It is interesting to note that, due to the difference in the frequency value, the $\text{Re}\{f_{\text{CM}}\}$ value relative to MDA-MB-231 cells in this second simulation (equal to 0.378) is lower than in the first simulation (equal to 0.643), so the standard DEP forces are, on the average, less intense this time.

In the first simulation, in which only MDA-MB-231 cells are present, all cells monotonically reduce their altitude over time, due to gravity and electromagnetic forces (p-DEP). It is important to note that in this second simulation two MDA-MB-231 cells, precisely the ones that have higher positions,

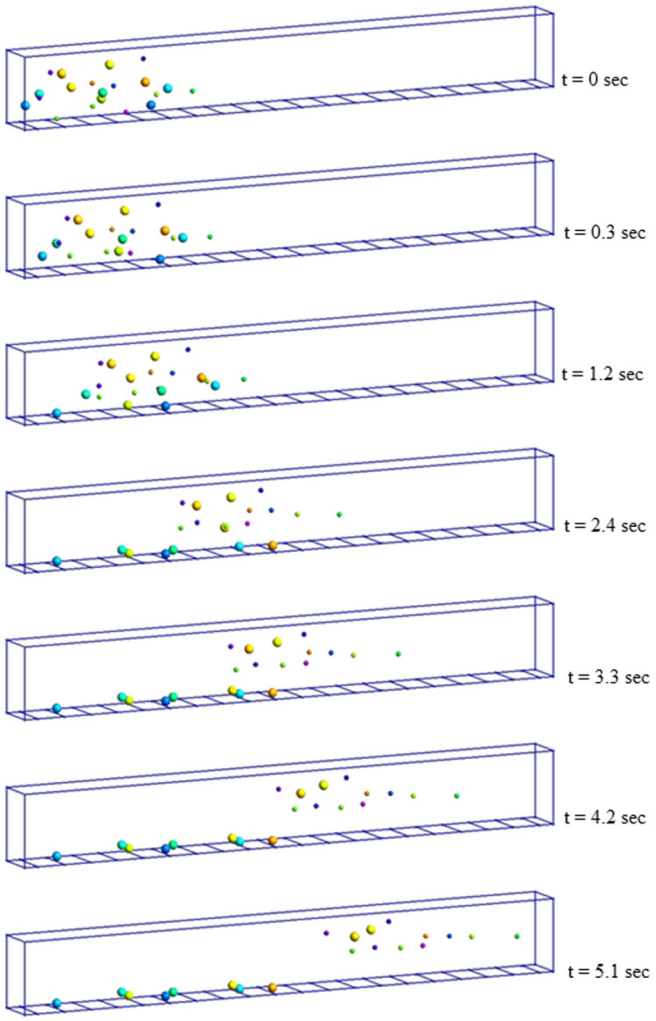

FIG. 11. Snapshots of simulated system (ten MDA-MD-231 cells and ten B-lymphocytes in a flowing colloidal solution) for $t = 0$, 0.3, 1.2, 2.4, 3.3, 4.2, 5.1 s (from upper to lower). The dimensions of the microchannel are $(800 \times 60 \times 100)$ μm^3 (for the length, depth, and height, respectively) and the number of electrodes is ten.

do not reduce elevation monotonically. Analyzing the numerical values of the z coordinate for each time cycle, we notice that in some time periods (for example, around $t = 3.5$ s) the height of these two particles increases slightly. This behavior is due to particle-particle interactions involving these two MDA-MB-231 cells and some B-lymphocytes that are in their spatial proximity. The B-lymphocytes are rejected by the bottom of the device (n-DEP) and they in turn push the MDA-MB-231 cells away from the electrodes. In order to quantify this effect, we analyze in detail the motion of the particle with the highest altitude during the entire simulation. Figure 12 shows the z coordinate of this particle as a function of the time in one of the time intervals in which a nonmonotonic variation of its height is provoked by the interaction with the n-DEP-type cells. The graph shows values taken at regular intervals of 0.06 s.

To highlight this phenomenon, we carried out an additional simulation similar to that of Fig. 5 (relative to a pair of

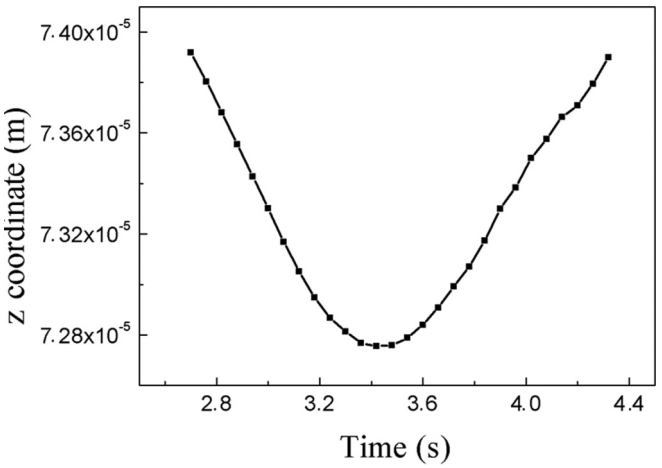

FIG. 12. z Coordinates of the particle with the highest altitude during the entire simulation, in a time interval where it presents a nonmonotonic change in altitude.

B-lymphocytes), in which there are one MDA-MB-231cell and one B-lymphocyte. The frequency is 10^5 Hz (MDA-MB-231 in p-DEP, B-lymphocytes in n-DEP), as in the previous simulation. The results are shown in Fig. 13, for time values equal to those of Fig. 5. We note that the particles repel each other, contrary to the case of Fig. 5, where two identical particles in p-DEP conditions attract, forming a chain.

It is important to note that also in this case particle-particle interactions are appreciable thanks to the use of the MST. A calculation of the dielectrophoretic force carried out using the standard DEP force [Eq. (11)] would not have detected this effect and therefore the two MDA-MB-231 higher positioned would have the same "qualitative" behavior as the others. Standard DEP force utilization could therefore overestimate the capture or separation efficiency of real devices.

VIII. CONCLUSIONS

In this manuscript, we propose the coupled MD-FEM technique as a tool for the study of the kinetics of systems

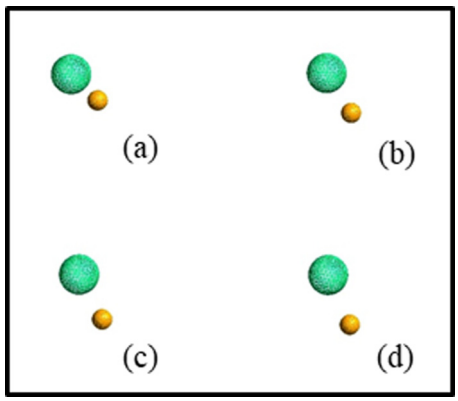

FIG. 13. Snapshots of simulation of one MDA-MD-231cell and one B-lymphocyte in a parallel flat face capacitor for $t = 0$, 0.1, 0.15, 0.21 s [(a–d), respectively]. Contrary to the case of Fig. 5, the particles repel each other.

where many-body particle-particle interactions are mediated by continuum fields, which evolve self-consistently with the system configuration. The presence of field-mediated forces cannot be exclusive. Indeed, in the systems we have specifically analyzed, the particles are also subjected to forces which can be rightly described using the particlelike formulation of the usual MD approach: In this manuscript we have also considered, in addition to the electromechanical forces, both single particle interactions (drag, lift, gravity) and two particle interaction (steric interaction). In the MD-FEM implementation of this research work, consolidated solvers (GMSH and FENICS) applying the finite-element-method technique for the PDE numerical solutions are integrated in the MD algorithm for the explicit integration of particle equations of motion.

As an explicit application of the method, we carried out simulations of the kinetics of cells (MDA-MB-231 tumor cells, B-lymphocytes, and mixtures of them) in a colloidal solution that flows through a microfluidic channel. In this case, the MD method finds application away from the atomistic simulation area. The field-mediated interactions are DEP forces generated by electrodes loaded with ac currents and calculated using the Maxwell stress tensor formalism. Using conventional concepts of p-DEP or n-DEP (DEP attraction or repulsion of cells towards the electrodes), we demonstrated that quantitative estimates and qualitative phenomenology of the system evolution can be correctly addressed only with our accurate methodology.

In the case of p-DEP only (i.e., a colloidal solution of the MFA-MB-231 cells only), the cells experience an attractive force that traps them close to the electrodes' edges. However, the particle-particle interactions strongly affect the trapping efficiency and, in general, the overall system evolution, leading also to the formation of complexes of cells (chains) moving as a single object after the cells merge due to attractive dipole-dipole interactions.

A simulation of a colloidal solution composed of MDA-MB-231 and B-lymphocytes was also presented. Due to the particular value of the chosen ac frequency, the first cell type experienced p-DEP and the second n-DEP, allowing studying the cell capture or separation capability of the simulated device. In the discussion of this particular simulation, we evidenced some effects that can be reproduced only by using nonapproximate methods for the calculation of electromagnetic forces.

An extension of our method in the DEP field could be planned in future works in order to generalize the particle shape (as the spherical approximation could be too stringent) and, consequently, to simulate the inner motion of electromechanical particles due to torques. Another natural application of the method is for magnetophoretic particles where similar issues as in the DEP arise [59,60] and particle-particle interactions that are important for the system dynamics [61] are often neglected in the theoretical analysis [62]. Moreover, the method can be easily adapted for the numerical evaluation of the medium kinetics, self-consistently solving a Navier-Stokes-type equation. In general, we note that a similar continuum-particle approach can be also formulated and implemented to other problems where the conventional force evaluation method used in MD is not applicable or its application is not computationally efficient (e.g., evolution of clusters of bonded particles, interaction between extended defects mediated by a strain field, mesoscopic systems, multiscale simulations, etc.).

[1] T. B. Jones, *Electromechanics of Particles* (Cambridge University Press, Cambridge, 2005).
[2] H. A. Pohl, J. Appl. Phys. **22**, 869 (1951).
[3] J. Castillo, S. Tanzi, M. Dimaki, and W. Svendsen, Electrophoresis **29**, 5026 (2008).
[4] M. Duchamp, K. Lee, B. Dwir, J. W. Seo, E. Kapon, L. Forro, and A. Magrez, ACS Nano **4**, 279 (2010).
[5] Y. Shen, E. Elele, and B. Khusid, Electrophoresis **32**, 2559 (2011).
[6] B. Cetin and D. Li, Electrophoresis **32**, 2410 (2011).
[7] T. B. Jones, IEEE Eng. Med. Biol. Mag. **22**, 33 (2003).
[8] P. R. C. Gascoyne, J. Noshari, T. J. Anderson, and F. F. Becker, Electrophoresis **30**, 1388 (2009).
[9] J. Cao, P. Cheng, and F. Hong, J. Electrost. **66**, 620 (2008).
[10] M. Sancho, V. Giner, and G. Martinez, Phys. Rev. E **55**, 544 (1997).
[11] A. La Magna, M. Camarda, I. Deretzis, G. Fisicaro, and S. Coffa, Appl. Phys. Lett. **100**, 134104 (2012).
[12] R. Natu and R. Martinez-Duarte, Micromachines **7**, 217 (2016).
[13] B. Hwang, D. Lee, B. Kim, and J. Lee, J. Mech. Sci. Technol. **30**, 3749 (2016).
[14] D. Lee, D. Kim, Y. Kim, K. Park, E. Oh, Y. Kim, and B. Kim, J. Lab. Autom. **19**, 60 (2014).
[15] M. Camarda, S. Scalese, and A. La Magna, Electrophoresis **36**, 1396 (2015).
[16] O. E. Nicotra, A. La Magna, and S. Coffa, Appl. Phys. Lett. **95**, 073702 (2009).
[17] X. Wang, X. B. Wang, and P. R. C. Gascoyne, J. Electrost. **39**, 277 (1997).
[18] M. P. Allen, Introduction to molecular dynamics simulation, in *Computational Soft Matter*, NIC Series Vol. 23, edited by N. Attig, K. Binder, H. Grubmüller, and K. Kremer (John von Neuman Institute for Computing, Jülich, Germany, 2004).
[19] https://www.fenicsproject.org/.
[20] J. D. Jackson, *Classical Electrodynamics* (Wiley, New York, 1978).
[21] L. D. Landau and E. M Lifshitz, *Electrodynamics of Continuous Media* (Pergamon Press, Oxford, 1984).
[22] A. M. Benselama, P. Pham, and P. Atten, J. Electrost. **64**, 437 (2006).
[23] S. Kumar and P. J. Hesketh, Sens. Actuators, B **161**, 1198 (2012).
[24] D. Lee, C. Yu, E. Papazoglou, B. Farouk, and H. M. Noh, Electrophoresis **32**, 2298 (2011).
[25] H.-H. Yi, Chin. J. Phys. **52**, 174 (2014).
[26] A. Gonzalez, A. Ramos, H. Morgan, N. G. Green, and A. Castellanos, J. Fluid Mech. **564**, 415 (2006).

[27] J. B. McLaughlin, Phys. Fluids A **1**, 1211 (1989).
[28] F. Aldaeus, Y. Lin, J. Roeraade, and G. Amberg, Electrophoresis **26**, 4252 (2005).
[29] A. Rosenthal and J. Voldman, Biophys. J. **88**, 2193 (2005).
[30] P. S. Williams, T. Koch, and J. Giddings, Chem. Eng. Commun. **111**, 121 (1992).
[31] https://www.bitbucket.org/mdfenics/md-fenics/src/master/.
[32] http://gmsh.info/.
[33] L. Verlet, Phys. Rev. **159**, 98 (1967).
[34] D. Frenkel and B. Smit, *Understanding Molecular Simulation* (Academic Press, New York, 2002).
[35] J. C. Phillips, R. Braun, W. Wang, J. Gumbart, E. Tajkhorshid, E. Villa, C. Chipot, R. D. Skeel, L. Kalé, and K. Schulten, J. Comput. Chem. **26**, 1781 (2005).
[36] W. Krauth, *Statistical Mechanics: Algorithms and Computations,* Oxford Master Series in Statistical, Computational, and Theoretical Physics (Oxford University Press, Oxford, 2006).
[37] J. Happel and H. Brenner, *Low Reynolds Number Hydrodynamics with Special Applications to Particulate Media* (Martinus Nijhoff Publishers, The Hague, Netherlands, 1983).
[38] K. Sangtae and J. K. Seppo, *Microhydrodynamics: Principles and Selected Applications* (Butterworth-Heinemann, Oxford, 1991).
[39] J. Zhang, K. Chen, and Z. H. Fan, Adv. Clin Chem. **75**, 12016.
[40] M. Sancho, G. Martinez, and C. Martin, J. Electrost. **57**, 143 (2003).
[41] P. Gascoyne, X. Wang, Y. Huang, and F. Becker, IEEE Trans Ind. Appl. **33**, 670 (1997).
[42] P. Gascoyne, C. Mahidol, M. Ruchirawat, J. Satayavivad, P. Watcharasit, and F. F. Becker, Lab Chip **2**, 70 (2002).
[43] P. Gascoyne, S. Shim, J. Noshari, F. F. Becker, and K. Stemke-Hale, Electrophoresis **34**, 1042 (2013).
[44] https://www.comsol.com/.
[45] S. Fan, C. Chiu, and P. Huang, Biomicrofluidics **4**, 043011 (2010).
[46] T. B. Jones, J. Electrost. **25**, 231 (1990).
[47] B. Yafouz, N. A. Kadri, and F. Ibrahim, in *Proceedings of the IEEE EMBS International Conference on Biomedical Engineering and Sciences* (IEEE, Piscataway, 2012), p. 118.
[48] J. Auerswald and H. F. Knapp, Microelectron. Eng. **67**, 879 (2003).
[49] F. F. Becker, X. B. Wang, Y. Huang, R. Pethig, J. Vykoukal, and P. Gascoyne, Proc. Natl. Acad. Sci. USA **92**, 860 (1995).
[50] Y. Huang, X. B. Wang, F. F. Becker, and P. R. Gascoyne, Biophys. J. **73**, 1118 (1997).
[51] K. Khoshmanesh, C. Zhang, F. J. T. Lopez, S. Nahavandi, S. Baratchi, K. Kalantar, and A. Mitchell, Electrophoresis **30**, 3707 (2009).
[52] M. S. Pommer, Y. Zhang, N. Keerthi, D. Chen, J. A. Thomson, C. D. Meinhart, and H. T. Soh, Electrophoresis **29**, 1213 (2008).
[53] L. S. Jang, P. H. Huang, and K. C. Lan, Biosens. Bioelectron. **24**, 3637 (2009).
[54] H. O. Fatoyinbo, N. A. Kadri, D. H. Gould, K. F. Hoettges, and F. H. Labeed, Electrophoresis **32**, 2541 (2011).
[55] M. P. Hughes and H. Morgan, J. Phys. D: Appl. Phys. **31**, 2205 (1998).
[56] D. F. Chen and H. Du, J. Micromech. Microeng. **16**, 1162 (2006).
[57] N. Crews, J. Darabi, P. Voglewede, F. Guo, and A. Bayoumi, Sens. Actuators, B **125**, 672 (2007).
[58] M. Camarda, G. Fisicaro, R. Anzalone, S. Scalese, A. Alberti A, F. La Via, A. La Magna, A. Ballo, G. Giustolisi, L. Minafra, F. P. Cammarata, V. Bravatà, G. I. Forte, G. Russo, and M. C. Gilardi, BioMed. Eng. OnLine **13**, 71 (2014).
[59] S. S. Leong, Z. Ahmad, and J. Lim, Soft Matter **11**, 6968 (2015).
[60] M. Benelmekki, L. M. Martinez, J. S. Andreu, J. Camachod, and J. Faraudo, Soft Matter **8**, 6039 (2012).
[61] J. Faraudo, J. S. Andreu, and J. Camacho, Soft Matter **9**, 6654 (2013).
[62] S. S. Leong, Z. Ahmad, J. Camacho, J. Faraudo, and J. Lim, J. Phys. Chem. C **121**, 5389 (2017).